PHYSICAL REVIEW A VOLUME 44, NUMBER 11 1 DECEMBER 1991

Electron loss at backward observation angles

Jianyi Wang, Carlos O. Reinhold, and Joachim Burgdörfer
Department of Physics, University of Tennessee, Knoxville, Tennessee 37996-1200
and Oak Ridge National Laboratory, Oak Ridge, Tennessee 37831-6377
(Received 10 June 1991)

A theoretical study of electron emissions resulting from ionzation of light hydrogenlike projectiles in ion (atom)-atom collisions with heavy targets is presented with emphasis on backward observation angles. Angular and energy distributions of the ejected electrons have been calculated with various approximation methods, which agree with or can be traced to the impulse approximation with the exact off-energy-shell transition amplitudes. Comparisons with experimental data have been made for collisions of H^0 and He^+ with Ar. We find good agreement for both the electron angular distributions and the angular variation of the peak position. Our results show that electron loss at backward angles is dominated by elastic scattering of the projectile electron in the strong field of the heavy target. A reliable representation of the potential and a high-order theory for scattering at this potential are required to describe the experiment accurately.

PACS number(s): 34.50.Fa, 34.10.+x, 34.80.Bm

I. INTRODUCTION

One of the fundamental processes occurring in ion (atom)-atom collisions is the ejection of electrons into the continuum. Study of the angular and energy distributions gives valuable information about the ionizing mechanisms and the atomic structure of the participants. Detailed comparison between experiment and theory using various projectiles and targets at different impact energies also provides sensitive tests of theoretical descriptions of the ionization process [1].

Electron emission becomes considerably complex and interesting when the impinging projectile carries electrons into the collision. In this case both target and projectile ionization contribute to the total electron spectrum. Furthermore, either of the collision partners can be ionized with the other either staying in the ground state or being excited to a discrete or continuum state.

The pioneering experimental studies were carried out by Burch, Wieman, and Ingalls [2] for heavy ion-atom collisions and by Wilson and Toburen [3] for molecular-ion–molecule collisions. A broad peak was discovered which was attributed to electrons emitted from the incident ions, frequently referred to as the electron-loss peak (ELP). It should be noted, however, that the dominant ionizing mechanisms that lead to the formation of the ELP are very different at either small or large angles. At forward angles the peak originates in a soft collision with the target and takes the form of a cusp at very small angles, i.e., the electron loss to the continuum (ELC) peak. On the other hand, the backward ELP is known to result from a head-on binary collision between a projectile electron and the target core.

The first treatment of projectile and target ionization in atom-atom collision was given by Bates and Griffing [4] using the first-order Born approximation. Burch, Wieman, and Ingalls [2] proposed a simple model for the ELP which assumed that projectile electrons scatter elastically at the target. The final distribution of electrons lost from the projectile is obtained by convoluting the elastic-scattering cross section over the Compton profile of the initial state of the projectile electron. This model was subsequently extended by Duncan and Menendez [5] using more realistic optical-model elastic-scattering cross sections and is often called the elastic-scattering model (ESM). Using a first-order Born approximation Drepper and Briggs [6] have stressed similarities between the ELP and target ionization with help of a Galilei transformation from the projectile rest frame to the laboratory frame. It has been shown, however, that the first-order Born approximation is insufficient for heavy targets [7] due to the strength of the perturbation. In this case a higher-order theory is necessary [8,9].

As first pointed out by Bates and Griffing [4] two independent channels contribute to projectile ionization in atom-atom collisions: the projectile electron can be knocked out by the screened target nucleus or by a target electron. The former is usually referred to as the singly inelastic (SI) channel since the target can (but not always) remain in its ground state. Similarly, the latter is referred to as the doubly inelastic (DI) channel since the target is excited or ionized. To the extent that these two channels lead to different final states they are to be added incoherently. A more precise definition of these channels is presented in Sec. II. Several calculations for electron loss [9,10] have included the DI channel in the first-order Born approximation. The relative importance of the two channels depends on the region in velocity space as well as the collision system.

Since the discovery of the ELP, ejected electron spectra have been measured for a variety of projectiles and targets by numerous authors [11–14]. One of the principal difficulties is the separation of the pure target ionization and of the projectile electron-loss components in the total yield of electrons. Recently developed coincidence techniques have aided in the understanding of the mecha-

nisms leading to target ionization and projectile electron loss [15,16].

The present work was motivated by an unresolved discrepancy between theory and experiment for the singly differential cross section (SDCS) for electron loss at backward angles in collisions of 0.5–0.8 MeV/u He^+ ions with He, Ne, and Ar targets [9,17]. Theoretical SDCS's have been found to be systematically smaller then their experimental counterparts by an amount that ranges from a factor of 2 to a factor of 4. The discrepancy is particularly intriguing considering the good agreement between theory and experiment at small angles where post-collisional distortions are much more important than at backward angles. Electron emission into large angles through a hard binary collision is thought to be one of the simplest mechanisms for ionization for which even classical binary encounter theory has been successfully applied [18].

Since the DI channel contribution to the cross section at backward angles can be shown to be negligible for *heavy targets* [9,19] our study concentrates on an improved treatment of the SI channel. The impulse approximation (IA) treats the scattering of the projectile electron in the strong target field to all orders. In line with previous investigations it serves as the starting point of our analysis. More specifically, we formulate an impulse approximation with the exact off-energy-shell transition amplitude in a time-dependent approach. By involving additional peaking and on-shell approximations we illustrate the relation of the exact impulse approximation to other models such as the ESM, the binary encounter approximation, and other on-shell impulse approximations. We find that for collisions involving heavy targets the cross sections for emission into large angles is very sensitive to the choice of the interaction potential and of the approach to the energy shell. We find the exact impulse approximation to be in good agreement with the experiment. Unless otherwise explicitly noted, atomic units (a.u.) $e=m_e=\hbar=1$ are used throughout the paper.

II. IMPULSE APPROXIMATION

We consider in the following the SI channel. The DI channel has been shown in the first-order Born approximation to be negligibly small at backward angles [9]. For heavy targets this remains true when higher-order Born terms are included [19]. We note, however, that for light targets electron-electron scattering contributions can no longer be neglected. It is important to realize that, in addition to the DI process caused by electron-electron scattering referred to in the following as the *correlated DI* process, there is a second, doubly inelastic process due to simultaneous projectile ionization and target excitation or ionization: independent but simultaneous projectile electron scattering at the screened target nucleus and target electron scattering at the screened projectile nucleus. We refer to this process in the following as the *uncorrelated DI* process. It should be noted that, within the limitations of the independent particle model [20], the uncorrelated DI process is approximately included in the perturbative calculation of the SI channel. If we denote the probability for projectile ionization by $P_p(I)$ and the probability for target excitation to a final state n by $P_T(n)$, we have

$$P_p(I)=P_p(I)P_T(0)+P_p(I)\sum_{n\,(\neq 0)}P_T(n)\ , \tag{1}$$

where we denote the initial target state by 0. In the calculation of $P_p(I)$ the charge distribution of the target in its ground state is used. While this may be a crude approximation for a process involving also simultaneous target ionization with large energies of the ejected electron, Eq. (1) nevertheless shows that the uncorrelated DI processes, apart from the inaccuracy of the potential, are implicitly included in the SI channel within the independent particle model. Correlated DI processes due to electron-electron scattering, on the other hand, amount to a breakdown of the independent particle model and represent true scattering correlations [20].

We consider a hydrogenlike projectile of nuclear charge Z_P, mass M_P, and speed v incident on a target atom of nuclear charge Z_T and mass M_T. The geometry of the collision system is depicted in Fig. 1. We use the semiclassical approximation in which the internuclear motion is described classically and the electronic evolution quantum mechanically. This approximation is justified in view of the large reduced mass $\mu=M_PM_T/(M_P+M_T)$ and the corresponding small de Broglie wavelength $1/\mu v \ll 1$. Furthermore, the internuclear motion is approximated by a straight-line trajectory with $\mathbf{R}=\mathbf{b}+\mathbf{v}t$, where $\mathbf{b}$ denotes the impact parameter.

The exact transition amplitude is given by

$$a_{fi}(b)=-i\int_{-\infty}^{\infty}dt\,\langle\phi_f(t)|V|\psi_i^+(t)\rangle \tag{2}$$

where $\phi_f(t)$ is the final state of the ejected electron and $\psi_i^+(t)$ is the exact scattering wave function propagated from the initial state $\phi_i(t)$ with outgoing boundary conditions, V is the interaction of the projectile electron with the target. We replace the exact wave function $\psi_i^+(t)$ by its impulse approximation (IA),

$$\psi_i^+(t)=\int d\mathbf{q}\,\tilde{\phi}_i(\mathbf{q},t)\psi_q^+\ , \tag{3}$$

where $\tilde{\phi}_i(\mathbf{q},t)=\langle\mathbf{q}|\phi_i(t)\rangle$ is the momentum space representation of the initial state and $\psi_{\mathbf{q}}^+$ represents the scattered electron wave of initial momentum $\mathbf{q}$

$$(-\tfrac{1}{2}\nabla^2+V)\psi_{\mathbf{q}}^+=\tfrac{1}{2}q^2\psi_{\mathbf{q}}^+ \tag{4}$$

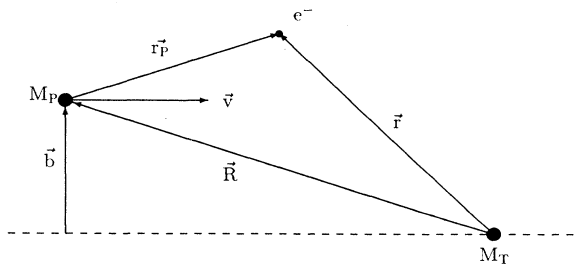

FIG. 1. Geometry of the collision system.

satisfying outgoing boundary conditions. $\psi_{\mathbf{q}}^{+}$ describes the exact propagation in the target potential V while the interaction with the projectile enters Eq. (3) only through its initial momentum distribution known as the Compton profile. Therefore the IA is expected to be valid for high impact speeds $Z_P/v \ll 1$, which is satisfied in our case for light projectiles $Z_P \approx 1$ at energies ≥ 0.5 MeV/u.

Substituting (3) into (2) and inserting a complete set of plane waves yields

$$a_{fi}^{\mathrm{IA}}(b) = -i \int dt\, d\mathbf{p}\, d\mathbf{q}\, \tilde{\phi}_f^{*}(\mathbf{p},t) \langle \mathbf{p}|V|\psi_{\mathbf{q}}^{+}\rangle \tilde{\phi}_i(\mathbf{q},t) , \tag{5}$$

where the integration limits are understood to extend over $\pm\infty$. In (5) the two-body T matrix element can be identified as

$$T_{fi}(\mathbf{p},\mathbf{q}) = \langle \mathbf{p}|V|\psi_{\mathbf{q}}^{+}\rangle , \tag{6}$$

which is the transition amplitude of a free electron with incident momentum $\mathbf{q}$ to a final momentum $\mathbf{p}$. In general $|\mathbf{q}| \neq |\mathbf{p}|$, i.e., (6) is off-energy shell and is not directly related to any physical observable.

After integration over time in (5) which gives rise to a δ function, we arrive at the exact transition amplitude in the IA,

$$a_{fi}^{\mathrm{IA}}(b) = -2\pi i \exp(i\mathbf{k}_f\cdot\mathbf{b}) \int d\mathbf{q}\, d\mathbf{p}\, \delta\left(\mathbf{q}\cdot\mathbf{v} - \frac{k_f^2+v^2-2\varepsilon_i}{2}\right) \exp(-i\mathbf{q}\cdot\mathbf{b}) T_{fi}(\mathbf{p}+\mathbf{v},\mathbf{p}+\mathbf{v}+\mathbf{q}-\mathbf{k}_f) \tilde{\varphi}_f^{-*}(\mathbf{p}) \tilde{\varphi}_i(\mathbf{p}+\mathbf{q}-\mathbf{k}_f) \tag{7}$$

with $\mathbf{k}_f$ being the ejected electron momentum in the laboratory frame and $\tilde{\varphi}_f^{-}(\mathbf{p})$ is the momentum space representation of the final continuum state given by an incoming Coulomb wave in the projectile rest frame with energy $\varepsilon_f = \frac{1}{2}(\mathbf{k}_f - \mathbf{v})^2$.

For electron emission into backward angles where $\mathbf{k}_f - \mathbf{v}$ is large, the Coulomb wave $\tilde{\varphi}_f^{-*}$ can be replaced by a plane wave. Independent numerical checks confirm the validity of this replacement near the ELP originally suggested by Drepper and Briggs [6]. The exact impulse approximation with plane-wave final states reduces to

$$a_{fi}^{\mathrm{IA}}(b) = -\frac{2\pi i}{v} \exp(i\mathbf{k}_f\cdot\mathbf{b}) \times \int d\mathbf{q}_\perp \exp(-i\mathbf{q}\cdot\mathbf{b}) T_{fi}(\mathbf{k}_f,\mathbf{q}) \tilde{\varphi}_i(\mathbf{q}-\mathbf{v}) \tag{8}$$

with $\mathbf{q} = \mathbf{q}_\perp + q_z^0 \hat{\mathbf{v}}$ and

$$q_z^0 = (k_f^2+v^2-2\varepsilon_i)/2v . \tag{9}$$

Without the replacement by a plane wave, the Fourier transformation of the initial state in Eq. (8), $\tilde{\varphi}_i$ should be replaced by the inelastic form factor

$$S_{fi}(\mathbf{p}) = \langle \varphi_f^{-}|\exp(-i\mathbf{p}\cdot\mathbf{r}_P)|\varphi_i\rangle . \tag{10}$$

$S_{fi}(\mathbf{p})$ should be used at small angles or small energies of the ejected electron. From (8) we find the doubly differential cross section (DDCS) as a function of the energy and angle of ejected electrons

$$\frac{d^2\sigma^{\mathrm{IA}}}{dE\, d\Omega} = \frac{16\pi^4}{v} k_f \int d\mathbf{q}\, \delta\left(\mathbf{q}\cdot\mathbf{v} - \frac{k_f^2+v^2-2\varepsilon_i}{2}\right) \times |T_{fi}(\mathbf{k}_f,\mathbf{q}) \tilde{\varphi}_i(\mathbf{q}-\mathbf{v})|^2 . \tag{11}$$

We refer in the following to (8) and (11) as the exact impulse approximation (in spite of the approximation of the liberated electron by a plane wave) since it contains the exact off-shell two-body T matrix element. Further frequently used approximation can now be derived from (8) and (11) by invoking various forms of on-shell approximations. The underlying idea in each case is that the on-shell T matrix element $|T_{fi}|^2$ becomes proportional to the elastic cross section for the scattering of an electron at the target core. The approach to the energy shell is not unique and as will be shown below, leads to discrepancies at backward angles.

Frequently employed on-shell approximations (OSA's) include the following choices.

(a) The form of OSA to (11) recently introduced by Hartley and Walters [9] consists of keeping the exact momentum transfer $\mathbf{q}-\mathbf{k}_f$ and choosing an approximate energy according to $E = \max(k_f^2/2, q^2/2)$. This choice of E ensures that the largest possible momentum transfer for a given pair $(\mathbf{k}_f,\mathbf{q})$ is less than $2\sqrt{2E}$, a relation satisfied in elastic scattering with well-defined energies. The T matrix element in (11) is therefore replaced by

$$16\pi^4 |T_{fi}(\mathbf{k}_f,\mathbf{q})|^2 \equiv \sigma_{\mathrm{el}}(E, \cos(\theta_{\mathrm{eff}})) , \tag{12}$$

where the effective scattering angle for elastic scattering θ_{eff} is given by

$$\cos(\theta_{\mathrm{eff}}) = 1 - |\mathbf{q}-\mathbf{k}_f|^2/4E . \tag{13}$$

It should be noted that the effective scattering angle resulting from the imposed constraints on E and on the momentum transfer is related to the true scattering angle $\theta = \cos^{-1}(\hat{\mathbf{q}}\cdot\hat{\mathbf{k}}_f)$ as follows:

$$\begin{aligned} &\sin^2(\theta_{\mathrm{eff}}/2) - \sin^2(\theta/2) \\ &\quad = (a^2+b^2-2ab\cos\theta)/4a^2 - \sin^2(\theta/2) \\ &\quad = -(a-b)(a+b-2a\cos\theta)/4a^2 , \end{aligned} \tag{14}$$

where $a = \max(q,k_f)$ and $b = \min(q,k_f)$. For backward scattering angles ($\theta \geq \pi/2$), $\sin^2(\theta_{\mathrm{eff}}/2) - \sin^2(\theta/2)$ is always negative and since $\sin^2(\theta/2)$ is a monotonically increasing function for $0 \leq \theta \leq \pi$, the effective angle is smaller, i.e., $\theta_{\mathrm{eff}} \leq \theta$. Finally the DDCS is given by

$$\frac{d^2\sigma}{dE\, d\Omega} = \frac{k_f}{v^2} \int d\mathbf{q}_\perp \sigma_{\mathrm{el}}(E, \cos(\theta_{\mathrm{eff}})) |\tilde{\varphi}_i(\mathbf{q}-\mathbf{v})|^2 . \tag{15}$$

(b) An alternative OSA can be devised by noting that the momentum distribution (i.e., the Compton profile) is strongly peaked around $\mathbf{q}\approx\mathbf{v}$ or $\mathbf{q}-\mathbf{v}\approx 0$. Therefore the energy-conserving δ function in (11) is modified such that

$$\delta(\mathbf{q}\cdot\mathbf{v}-vq_z^0)\approx\delta((q^2+v^2)/2-vq_z^0) . \quad (16)$$

This leads to a constraint in the magnitude of q of the form

$$q_0^2/2=k_f^2/2-\varepsilon_i . \quad (17)$$

Conservation of the exact momentum transfer $\mathbf{q}-\mathbf{k}_f$ requires the replacement of the off-shell T matrix in (11) by the elastic differential cross section

$$16\pi^4\frac{q_0}{v}|T_{fi}(\mathbf{k}_f,\mathbf{q})|^2\equiv\sigma_{\rm el}(q_0^2/2,\cos(\theta_{\rm eff})) \quad (18)$$

with

$$\cos(\theta_{\rm eff})=1-|\mathbf{q}_0-\mathbf{k}_f|^2/2q_0^2 . \quad (19)$$

The effective scattering angle in this approximation is related to the true scattering angle θ through

$$\sin^2(\theta_{\rm eff}/2)-\sin^2(\theta/2)$$
$$=-(q_0-k_f)(q_0+k_f-2q_0\cos\theta)/2q_0^2 . \quad (20)$$

As is the case in choice (a), the effective scattering angle is also smaller, i.e., $\theta_{\rm eff}\le\theta$. However since q_0-k_f is small [Eq. (17)] $\theta_{\rm eff}$ is closer to the true scattering angle than in (a). The DDCS is now of the form

$$\frac{d^2\sigma}{dE\,d\Omega}=k_f\int d\Omega_{q_0}\sigma_{\rm el}(q_0^2/2,\cos(\theta_{\rm eff}))|\tilde{\varphi}_i(\mathbf{q}_0-\mathbf{v})|^2 . \quad (21)$$

The physical picture underlying (21) is that the doubly differential cross section is determined by a subset of the Compton profile lying on a surface of constant q_0 [Eq. (17)], which is scattered into the direction of $\mathbf{k}_f$. We point out that the OSA scheme represented by Eq. (21) is essentially equivalent to the ESM proposed by Burch, Wieman, and Ingalls [2]. The only difference appears to be that the initial binding energy of the projectile electron is explicitly taken into account in Eq. (21).

(c) In the binary encounter approximation (BEA) originally proposed by Bonsen and Vriens [21] the direction of the outgoing electron $\hat{\mathbf{k}}_f$ rather than the momentum transfer is preserved. This implies the following replacement for the T matrix element in (11),

$$16\pi^4|T(\hat{\mathbf{k}}_f q,\mathbf{q})|^2\equiv\sigma_{\rm el}(q^2/2,\cos\theta) . \quad (22)$$

Unlike the two previous approximations the elastic cross sectioned depends on the true scattering angle. The energy conserving δ function in (11) is now replaced by $\delta(q^2/2-q'^2/2)$, where the energy $E=q'^2/2$ for elastic scattering is determined from the relation for an impulsive momentum transfer in the projectile field

$$(\mathbf{k}_f-\mathbf{v})^2/2=(\mathbf{q}'-\mathbf{v})^2/2-(\mathbf{q}-\mathbf{v})^2/2+\varepsilon_i . \quad (23)$$

The latter has an obvious physical interpretation: the kinetic energy of the scattered electron $(\mathbf{q}'-\mathbf{v})^2/2$, as seen in the projectile rest frame, must be equal to the asymptotic kinetic energy $(\mathbf{k}_f-\mathbf{v})^2/2$ after escaping from the projectile potential with a local value at the point of the collision, $V(r)=\varepsilon_i-(\mathbf{q}-\mathbf{v})^2/2$.

The corresponding BEA cross section is given by

$$\frac{d^2\sigma^{\rm BEA}}{dE\,d\Omega}=\frac{k_f}{v}\int d\mathbf{q}\,\sigma_{\rm el}(q^2/2,\cos\theta)|\tilde{\varphi}_i(\mathbf{q}-\mathbf{v})|^2$$
$$\times\delta(q^2/2-q'^2/2) . \quad (24)$$

Defining $\mathbf{p}=\mathbf{q}-\mathbf{v}$ a simpler expression for the cross section can be obtained by integrating (24) over the angle $\cos\theta_p=\hat{\mathbf{p}}\cdot\hat{\mathbf{v}}$,

$$\frac{d^2\sigma^{\rm BEA}}{dE\,d\Omega}=\frac{k_f}{v^2}\int_{p_{\rm min}}^{p_{\rm max}}dp\,p|\tilde{\varphi}_i(\mathbf{p})|^2$$
$$\times\int_0^{2\pi}d\phi\,\sigma_{\rm el}(q'^2/2,\cos\theta) , \quad (25)$$

where ϕ is the azimuthal angle of $\mathbf{p}$ (or $\mathbf{q}$) and $p_{\rm min}$ and $p_{\rm max}$ are the minimum and maximum values for which Eq. (23) can be satisfied. It is important to note that $\sigma_{\rm el}(q^2/2,\cos\theta)$ is not axially symmetric with respect to $\hat{\mathbf{v}}$ and is therefore ϕ dependent.

III. ELASTIC SCATTERING IN THE TARGET POTENTIAL

Since both the exact two-body T matrix element as well as its on-shell approximations determine the behavior of the electron-loss cross section we have investigated the elastic electron scattering in the effective target potential in detail. In our calculation we have used a parametrized model potential [22] for the static potential of the Ar target. We have tested this model potential by comparing it with the electrostatic potential calculated with the Hartree-Fock method. For $r\le 2$ they are virtually identical. Since at backward angles the small-r region is most important, it is therefore appropriate for our purposes. The calculation of the exact scattered wave [Eq. (4)] proceeds most easily with the help of a partial-wave expansion. The resulting elastic-scattering cross section for electrons on argon can be tested by comparison with experimental data. In Fig. 2 we display the elastic cross section for electrons on Ar with a typical energy of 200 eV. The calculation with the effective potential is seen to agree within 20% with experimental values. It indicates that exchange effects are small in 0.5 MeV/u energy range [24].

One characteristic feature of the scattering cross section is a rise at large angles ($\theta\ge 130°$). Since this structure will eventually survive the convolution with the Compton profile [Eq. (11)] it is important to understand its origin. Figure 3 displays the decomposition of the total elastic cross section into partial-wave components. The rapid decrease with l is characteristic for heavy neutral targets. For small l (or impact parameter b) the electron is influenced by a strong, only slightly screened, Coulomb potential. For moderately high l, however, the electron interacts with an essentially neutral target with which the interaction is, apart from polarization forces,

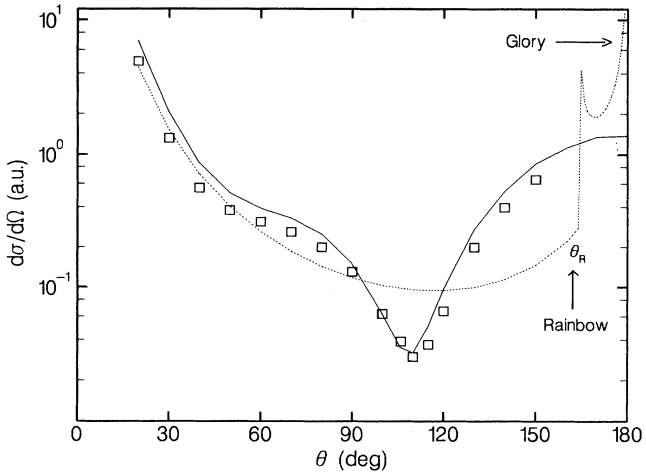

FIG. 2. Quantum and classical cross section for elastic scattering of 200-eV electrons at Ar. (——) quantum-mechanical result; (— — —), classical result; (□) experimental data of Ref. [23]. The classical curve shows a rainbow near $\theta_R \sim 160°$ and a glory near 180° [see text, Eq. (26), for definitions of rainbow and glory].

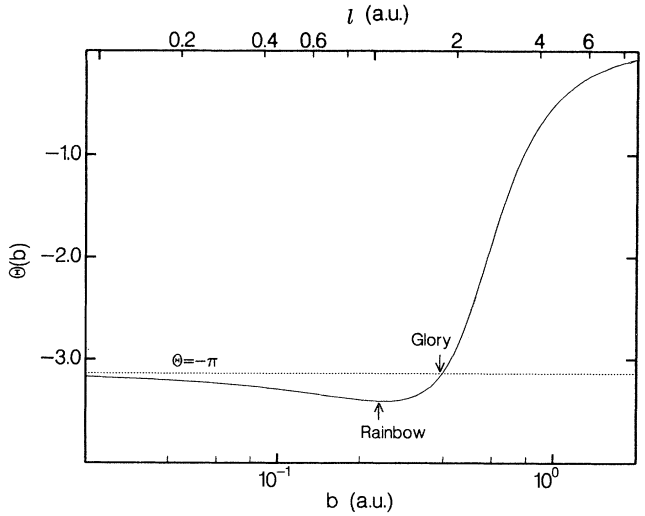

FIG. 4. Classical deflection function for elastic scattering of 200-eV electrons by Ar. The rainbow occurs at an impact parameter $b \simeq 0.2$, corresponding to an angular momentum of $l \sim 1$. The glory is around $b \simeq 0.4$, where the curve crosses $\theta = -\pi$.

negligible. The fact that only a few partial waves effectively contribute results in the oscillatory structures in the elastic differential cross section. In fact, in a simplified model with partial-wave contributions only from $l=0$ and $l=2$, the angular distribution reflects the nodal structure of the Legendre polynomial P_2 with minima at $\theta \approx 54°$ and 126° and maxima at 0°, 90°, and 180°. The latter accounts qualitatively for the structures seen in Fig. 2.

These structures are to be distinguished from classical rainbow and glory singularities present in the classical cross section also shown in Fig. 2. Their origin can be traced to the classical deflection function shown in Fig. 4.

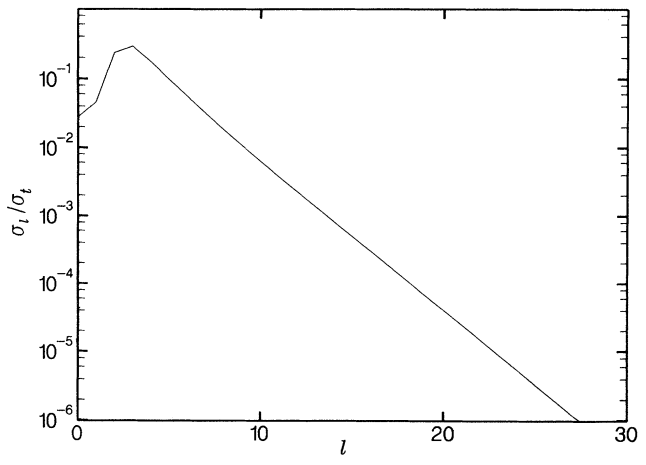

FIG. 3. Partial-wave decomposition of elastic cross section for 200-eV electrons on Ar. Each partial-wave contribution σ_l is normalized to the total cross section σ_t.

Recalling that the classical cross section is given by

$$\frac{d\sigma}{d\Omega} = \frac{1}{\sin\theta} \sum_i b_i \left| \frac{db_i}{d\Theta} \right| , \tag{26}$$

where i runs through all impact parameters contributing at a given observation angle θ, it is seen that a singularity can occur if either $d\Theta/db$ or $\sin\theta$ is zero. The former gives rise to a rainbow, the latter to a glory. In the neighborhood of the rainbow or the glory, there are three impact parameters leading to the same θ (see Fig. 4). Since $\theta(b \to \infty) = 0$ and $\theta(b \to 0) = -\pi$, the occurrence of a rainbow for fast electron-atom collisions requires the decrease of the deflection function to below $-\pi$ at finite impact parameters. The prerequisite for the latter is a locally strong attractive potential as can be found near the nucleus of a heavy target. Thus, the strong variation of the target potential is the origin of both the quantum interference of a limited number of partial waves and of the classical rainbow. However the rise of the cross section is not a classical rainbow or a glory. In order to investigate the relation between the quantum-mechanical and classical scattering cross section we have tested a semiclassical approximation [25] that remains valid when the rainbow is close to π and overlaps with the glory. The results do not agree with the exact cross section in either shape or magnitude. In tracing the discrepancy we found that the first step of a semiclassical approximation, the replacement of the exact scattering phases by their WKB limit is valid, i.e., the resulting cross section agrees to a very good approximation with the exact quantum-mechanical result. The latter implies that the De Broglie wavelength is still sufficiently small compared to the characteristic spatial variation of the potential. The breakdown of the semiclassical approximation occurs in the second step:

the replacement of the sum over partial waves by an integral over l (or b). The latter is an obvious consequence of the fact that only a few partial waves contribute.

We conclude that the enhancement seen at backward angles is a pure quantum-mechanical effect that can be traced to the fact that the cross section in Fig. 2 can be reproduced with very few partial waves. We note that due to the presence of classical singularities in the elastic cross section, classical methods should be used with caution for calculating electron-loss cross section for heavy targets. Furthermore, classical (or semiclassical) rainbow and glory structures will be reflected in the quantum-mechanical cross section when the deflection function for fast electrons resembles the one shown in Fig. 4 and, in addition, the range of impact parameters contributing to the rainbow and glory encompasses a wide range of angular momenta.

IV. RESULTS AND DISCUSSION

A. Doubly differential cross sections (DDCS's)

In this section we present results for H^0 and He^+ on Ar. Argon was chosen to be representative of heavy targets because of the availability of experimental data for these collision systems. We first consider 0.5-MeV atomic hydrogen incident on Ar. Calculations of the doubly differential cross section (DDCS) for the SI channel at 130° and 150° are compared in Fig. 5 with recent measurements by Heil [16]. A single, broad peak is observed and identified as the electron loss or binary peak resulting from projectile ionization. The shape of the ELP is nearly symmetric reflecting to a certain extent the Compton profile of the projectile initial state [H(1s)]. Even though the widths and positions of the ELP at the two angles are similar there is a large difference in the peak height. The ELP at 150° is almost twice as high as at 130°. This can be qualitatively understood by noting that the elastic cross section (Fig. 2) increases with angle in the backward direction. Overall, the agreement between theory and experiment is very good considering that the experimental data are absolute and no normalization factors are used in the comparison. At both angles the agreement with experiment is better on the higher-energy side of the ELP than on the lower side. The latter is partly due to increasing target ionization contributions at lower energies. Another source could be the absence of the correlated DI channel in the theory.

The above calculation has been performed using the full off-energy-shell T matrix elements (11). In Fig. 6 we compare the various on-shell approximations we discussed in Sec. II with the exact impulse approximation for DDCS at 135° for He^+ on Ar at 0.8 MeV/u. We note that the calculation of Ref. [9] shown in Fig. 6 includes the correlated DI channel in first-order Born approximation. However, since the latter has been shown to be small at backward angles, this inconsistency does not distort the comparison. Furthermore, since the experimental data are relative we have adapted the normalization of Ref. [9] for the SDCS. While the different on-shell approximations (curves a and b in Fig. 6) reproduce the shape of the ELP we find remarkable differences in the magnitude of the cross section. Obviously, the DDCS at backward angles is extremely sensitive to the on-shell approximations used. Again, its origin can be traced to the strong rise of the elastic-scattering cross section at backward angles (Fig. 2). Since an on-shell approximation amounts, in a simplified picture, to an alteration of either the exact momentum transfer vector or the final momentum vector, one probes, in effect, the elastic cross section at different backward angles. In line with this analysis we find the DDCS at forward angles, i.e., smaller momentum transfers, is much less sensitive to choice of the on-shell approximation. In view of the simplicity of the OSA given by Eq. (21) (curve b) and its good agreement with the exact off-shell IA (curve d), we use this model for the

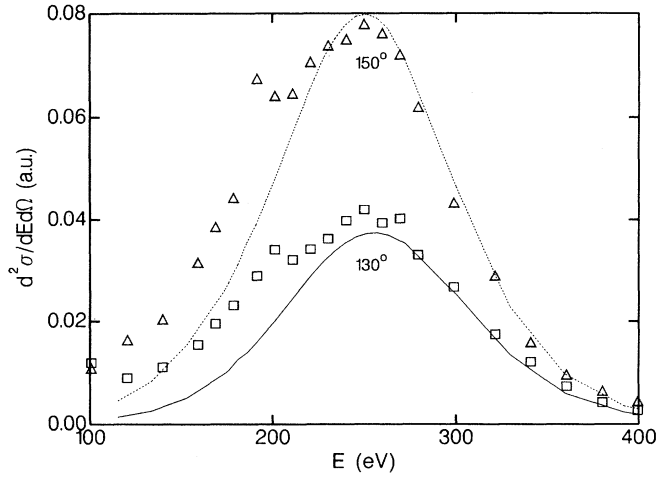

FIG. 5. Absolute DDCS for H^0+Ar at 0.5-MeV/u calculated with the off-shell IA. (——) 130° (— — —) 150°. Experimental data from Ref. [16]; (□) 130°; (△) 150°.

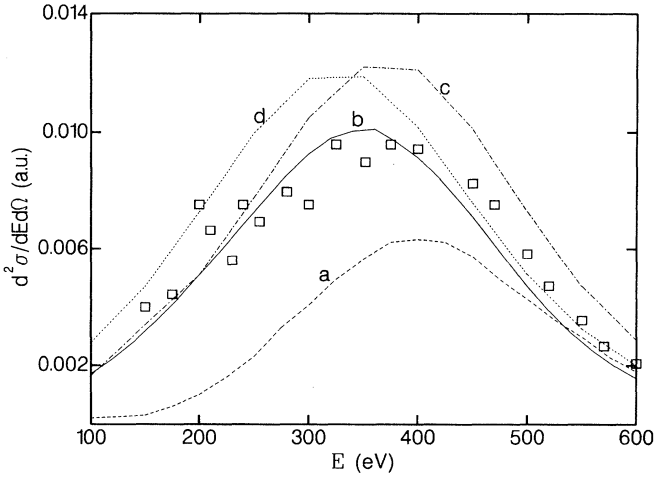

FIG. 6. DDCS for He^++Ar at 0.8-MeV/u. (a) On-shell IA from Ref. [9] [Eq. (15)]; (b) on-shell IA [Eq. (21)]; (c) BEA [Eq. (25)]; (d) off-shell IA [Eq. (11)] (see text). (□) experimental data from Ref. [14] normalized to our result.

calculation of the SDCS and the peak position presented below.

B. Singly differential cross sections (SDCS's)

The angular distribution of loss electrons, i.e., the singly differential cross section (SDCS) is obtained by integrating the DDCS over all electron energies. Figure 7 displays the SDCS for H^0 and He^+ on Ar at 0.5 -MeV/u. The most important observation is that the SDCS closely resembles the elastic cross section. The rise at large angles following a minimum around 110° is seen to be present for both H^0 and He^+ projectiles. In addition, the magnitude for the two collision systems seems to be equal within experimental error bars although the theoretical calculations show that the SDCS is slightly higher for H^0 than for He^+. The similarity in both shape and magnitude can be viewed as a direct experimental confirmation of the validity of the impulse approximation. Apart from the different width of the Compton profile, the loss cross section should be independent of the projectile and only determined by the interaction with the heavy target. Furthermore, the good agreement of the IA with the experiment with only the SI channel included confirms that the correlated DI channel is, indeed, negligible. Previous discrepancies are due to the choice of on-shell approximations rather than to an inadequate representation of the DI channel. Clearly, since only first-approximation Born calculations are available for the DI channel at backward angles more elaborate calculations including higher-order contributions should be performed before arriving at a more definitive conclusion.

C. Angular dependence of the peak position

It has been experimentally observed [17] that the dependence of the position in energy of the ELP on the ejection angle is nonmonotonic. The peak position is found to be shifted to energies below the position expected for a binary encounter collision of a heavy particle with a free electron of well-defined momentum. This is due to the binding energy effect and to the convolution of the Compton profile with a rapidly decreasing elastic cross section as a function of energy. This shift is displayed in Fig. 8 for the case of He^+ on Ar at 0.5 MeV/u for which we find qualitative agreement between experiment and theory. We note that the peak position displays a hump around 110°, i.e., the shift is reduced by a factor of ~ 2. This angle is found to correspond to the minimum of the SDCS (Fig. 7), which in turn is related to the minimum of the elastic cross section. We therefore analyze the dependence of the elastic cross section on the electron energy around this angle as depicted in Fig. 9. The 110° curve shows a minimum due to the strong partial-wave interference at an energy below the free electron energy $v^2/2$. In contrast, the cross section decreases monotonically from intermediate to large electron energies, as intuitively expected. The net effect is a reduction of the cross section on the low-energy tail and an enhancement on the high-energy tail, and hence, a partial suppression of the peak shift to lower energies at $\theta \approx 110°$.

The increase of the peak shift (Fig. 8) at large angles reflects the fact that the slope of the elastic cross section (Fig. 9) as a function of k (or E) becomes steeper with increasing E, such that the opposite trend becomes operative: The high-energy tail of the ELP is reduced relative to the low-energy tail resulting in an increased peak shift.

The anomalous energy dependence of elastic cross section seen in the 110° curve in Fig. 9 has interesting implications for heavier targets. First, the same behavior is expected to be found at more than one angle since more minima in the elastic cross sections are present [26], which Duncan and Menendez have indeed observed for H^-, $He^+ + Kr$ collisions [27]. Furthermore, as the target becomes heavier the minimum (as a function of energy)

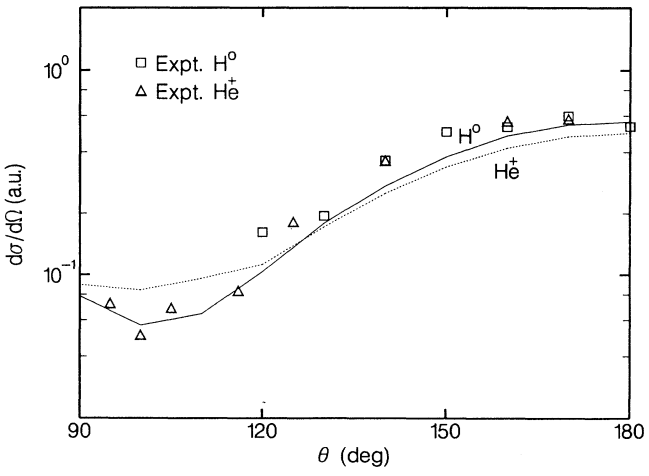

FIG. 7. SDCS for H^0 (——); He^+ (— — —)+Ar at 0.5 MeV/u. Experimental data, H^0 from Ref. [16]; He^+ from Ref. [17].

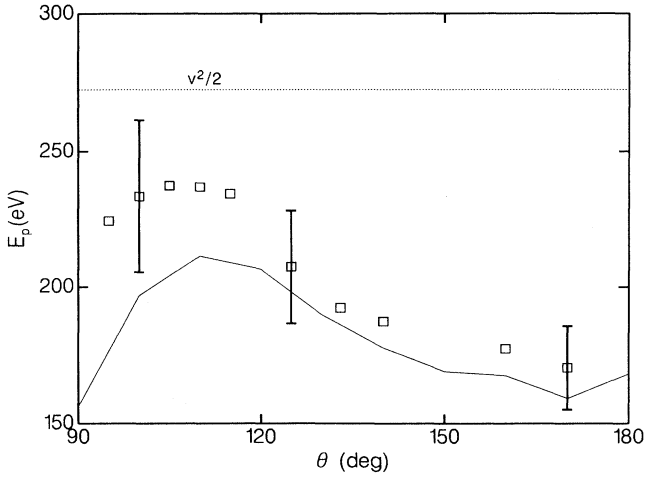

FIG. 8. Angular variation of the peak position E_p for $He^+ + Ar$ at 0.5 MeV/u. (□) experimental data of Ref. [17]. The free electron energy $v^2/2$ corresponds to 272 eV.

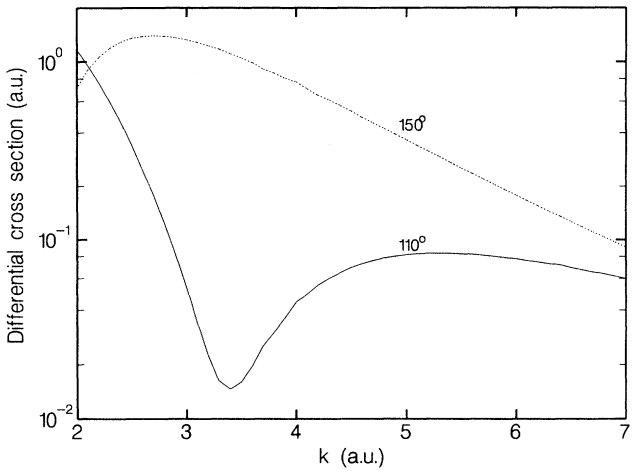

FIG. 9. Differential cross section for elastic scattering of electrons by Ar as a function of the incident momentum k. (——) 110°; (— — —) 150°.

becomes so sharp that it can "burn" a hole in the energy spectrum such that the DDCS would show two peaks instead of one. This phenomenon has been demonstrated experimentally and theoretically in a recent study of the forward-binary-peak splitting [28,29] by partially stripped heavy-ion impact. By the same token the enhancement seen at backward angles for electron loss is also reflected in the forward-binary-electron production where the magnitude of the cross section for partially stripped ion impact exceeds that for the fully stripped ion impact [30–32]. Our present study for electron loss at backward angles, coupled with the forward binary peak for target ionization, provides a unified description of the backward- and forward-binary-electron production mechanism, whose origin is largely dominated by the elastic scattering in the respective target or projectile fields.

V. CONCLUSIONS

Projectile electron loss at backward angles has been studied for heavy targets. Comparing experimental results with theoretical calculations using an impulse approximation with the exact off-energy-shell transition matrix elements, good agreement has been obtained for both the DDCS and the SDCS for H^0 impact of Ar. The calculated SDCS as well as the angular variation of the peak position for He^+ on Ar have also been found to be in good accord with experiment. It is therefore concluded that for heavy targets like Ar, the singly inelastic channel is the dominant ionizing channel at backward angles.

We find the properties of the electron emission spectrum to be largely governed by the elastic-scattering process at the heavy target. A reliable representation of the target potential and an accurate treatment of the two-body T matrix element for scattering in the target field is therefore a prerequisite for a successful description. The present analysis stresses the similarity in the underlying mechanism for electron loss at backward angles in collisions with heavy targets and for the target binary peak at forward angles in collisions with partially stripped heavy projectile ions.

We conclude by noting that the application of the present analysis to light targets does not account for the previously noted differences between theory and experiment. Evidently, other ionizing mechanisms play an important role. Work is in progress in this direction using (i) a second-order Born approximation for the correlated DI channel and (ii) a modified SI theory that can account for processes such as the transfer of a projectile electron to the continuum of the target.

ACKNOWLEDGMENTS

We would like to thank Dr. O. Heil for many fruitful discussions and for providing us with tabulated experimental data. We also would like to thank Dr. A. Köver for illuminating suggestions. This work was supported in part by the NSF and DOE under Contract No. DE-AC05-84OR21400.

[1] N. Stolterfoht, *Structure and Collisions of Ions and Atoms,* edited by I. A. Sellin, Topics in Current Physics Vol. 5 (Springer-Verlag, Berlin, 1978), pp. 155.
[2] D. Bruch, H. Wieman, and W. B. Ingalls, Phys. Rev. Lett. **30**, 823 (1973).
[3] W. E. Wilson and L. H. Toburen, Phys. Rev. A **7**, 1535 (1973).
[4] D. R. Bates and G. Griffing, Proc. Phys. Soc. London, Sect. A **67**, 663 (1954).
[5] M. M. Duncan and M. G. Menendez, Phys. Rev. A **19**,49 (1979).
[6] F. Drepper and J. S. Briggs, J. Phys. B **9**, 2063 (1976).
[7] H. R. J. Walters, J. Phys. B **8**, L54 (1975).
[8] D. H. Jakubassa, J. PHys. B **13**, 2099 (1980).
[9] H. M. Hartley and H. R. J. Walters, J. Phys. B **20**, 3811 (1987).
[10] J. S. Briggs and M. H. Day, J. Phys. B **13**, 4797 (1980).
[11] L. H. Toburen and W. E. Wilson, Phys. Rev. A **19**, 2214 (1979).
[12] M. E. Rudd, J. S. Risley, J. Fryar, and R. G. Rolfes, Phys. Rev. A **21**, 506 (1980).
[13] M. M. Duncan and M. G. Menendez, Phys. Rev. A **16**, 1799 (1977).
[14] A. Köver, D. Varga, Gy Szabó, D. Berényi, I. Kádár, S. Ricz, J. Végh, and G. Hock, J. Phys. B **16**, 1017 (1983).
[15] R. D. DuBois and S. T. Manson, Phys. Rev. Lett. **57**, 1130 (1986).
[16] O. Heil (private communication).
[17] A. Köver, Gy Szabo, L. Gulyás, K. Tökési, D. Berényi, O. Heil, and K. O. Groeneveld, J. Phys. B **21**, 3231 (1988).
[18] M. R. C. McDowell and J. P. Coleman, *Introduction to the Theory of Ion-Atom Collisions* (North-Holland, Amster-

dam, 1970).
[19] J. Wang, C. O. Reinhold, and J. Burgdörfer (unpublished).
[20] J. H. McGuire and L. Weaver, Phys. Rev. A **16**, 41 (1977).
[21] T. F. M. Bonsen and L. Vriens, Physica (Utrecht) **47**, 307 (1970).
[22] R. H. Garvey, C. J. Jackman, and A. E. S. Green, Phys. Rev. A **12**, 1144 (1975).
[23] R. D. DuBois and M. E. Rudd, J. Phys. B **9**, 2657 (1976).
[24] K. Taulbjerg, J. Phys. B **23**, L761 (1990), and references therein; Z. Chen, D. Madison, and C. D. Lin (unpublished).
[25] P. Pechukas, Phys. Rev. **181**, 166 (1969).
[26] I. E. McCarthy, C. J. Noble, B. A. Phillips, and A. D. Turnbull, Phys. Rev. A **15**, 2173 (1977).
[27] M. M. Duncan and M. G. Menendez, Phys. Rev. A **23**, 1085 (1981).
[28] C. Kelbch, S. Hagmann, S. Kelbch, R. Mann, R. E. Olson, S. Schmidt, and H. Schmidt-Böcking, Phys. Lett. A **139**, 304 (1989).
[29] C. O. Reinhold, D. R. Schultz, R. E. Olson, C. Kelbch, R. Koch, and H. Schmidt-Böcking, Phys. Rev. Lett. **66**, 1842 (1991).
[30] P. Richard, D. H. Lee, T. J. M. Zouros, J. M. Sanders, and J. L. Shinpaugh, J. Phys. B **23**, L213 (1990).
[31] C. O. Reinhold, D. R. Schultz, and R. E. Olson, J. Phys. B **23**, L591 (1990).
[32] R. Shingal, Z. Chen, K. R. Karim, C. D. Lin, and C. P. Bhalla, J. Phys. B **23**, L637 (1990).